

# Science Advances



[advances.sciencemag.org/cgi/content/full/2/5/e1501768/DC1](http://advances.sciencemag.org/cgi/content/full/2/5/e1501768/DC1)

## Supplementary Materials for

### Experimental river delta size set by multiple floods and backwater hydrodynamics

Vamsi Ganti, Austin J. Chadwick, Hima J. Hassenruck-Gudipati, Brian M. Fuller, Michael P. Lamb

Published 20 May 2016, *Sci. Adv.* **2**, e1501768 (2016)

DOI: 10.1126/sciadv.1501768

#### This PDF file includes:

- Supplementary Materials and Methods
- fig. S1. Idealized schematic of backwater and drawdown hydrodynamics.
- fig. S2. Instantaneous measurements of water and bed surface profiles along with the measured flow depth, depth-averaged flow velocity, and Froude number for experiment A.
- fig. S3. Instantaneous measurements of water and bed surface profiles along with the measured flow depth, depth-averaged flow velocity, and Froude number for both flows in experiment B.
- fig. S4. Photo sequence of the process of avulsion in experiment B.
- fig. S5. Temporal evolution of avulsion length in constant discharge delta.
- fig. S6. Water surface velocity across the backwater reach in constant discharge delta.
- table S1. Field data compilation of avulsion length and backwater length.
- Legends for movies S1 to S3
- References (53, 54)

#### Other Supplementary Material for this manuscript includes the following:

(available at [advances.sciencemag.org/cgi/content/full/2/5/e1501768/DC1](http://advances.sciencemag.org/cgi/content/full/2/5/e1501768/DC1))

- movie S1 (.mp4 format). Experimental evolution of constant discharge delta.
- movie S2 (.mp4 format). Experimental evolution of variable discharge delta.
- movie S3 (.mov format). Overhead dye video of the constant discharge delta.

## Supplementary Material and Methods

### Computation of avulsion length and backwater length for field-scale deltas

In Fig. 1 of the main text, we report on the measured avulsion length ( $L_a$ ) and the computed backwater length scale ( $L_b$ ) for the field-scale deltas. The following relation approximates the backwater length scale (e.g., 11, 18, 20):

$$L_b \sim h_c / S$$

where  $S$  is the channel bed slope, and  $h_c$  is the characteristic flow depth, which can be estimated by the following relation (53):

$$h_c = \left( \frac{c_f Q_c^2}{g w^2 S} \right)^{1/3}$$

where  $Q_c$  is the characteristic flow discharge (assumed equal to the flood of 2-year recurrence interval),  $w$  is the channel width,  $c_f$  is a bed friction coefficient, and  $g$  is gravitational acceleration. Chatanantavet *et al.* (18) report on the characteristic flow discharge, bed slopes, channel widths, and typical friction coefficients for alluvial rivers. Further, they also report on the streamwise distance of the avulsion nodes from the shoreline measured from satellite imagery. We reproduce their compilation here, which was used to produce Fig. 1 of the main text.

## Supplementary Figures

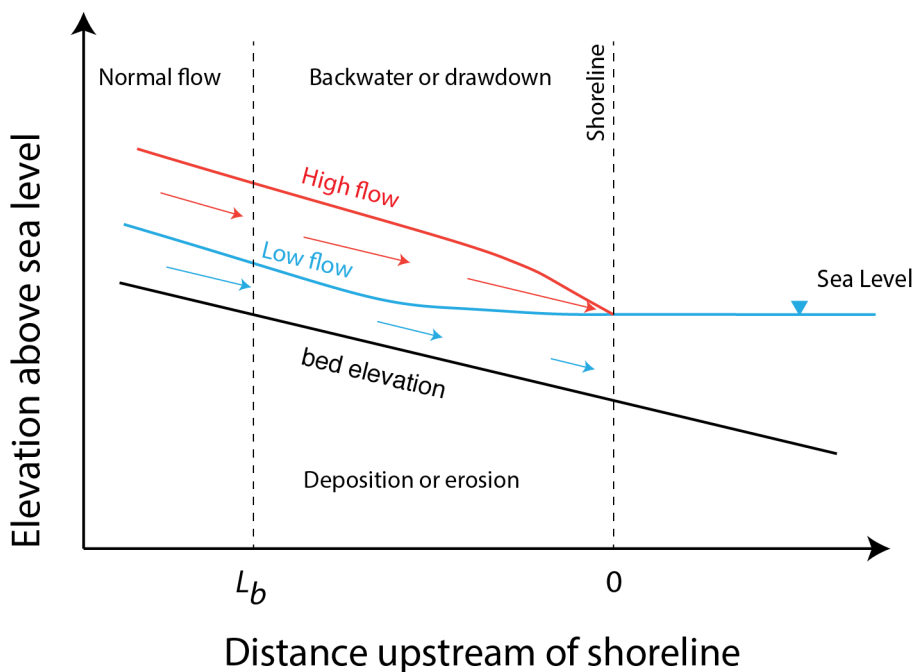


**fig. S1. Idealized schematic of backwater and drawdown hydrodynamics.** This plot shows a slope schematic of the longitudinal profiles of water surface elevation for a constant-width and constant-river entering an ocean. During low flow (blue curve), the flow decelerates, which causes sediment deposition within the backwater reach ( $0-L_b$ ). In contrast, during high flows (red curve), the water surface slope steepens; flow accelerates, which causes erosion in the lowest portions of the alluvial river (e.g., 18, 20, 30). Backwater and drawdown hydrodynamics are characterized by flow deceleration and acceleration (nonuniform flows), respectively, which do not prevail upstream in the normal flow reach. The water surface curvature shown in this schematic is only expected for the simple case of uniform width and constant bed-slope.

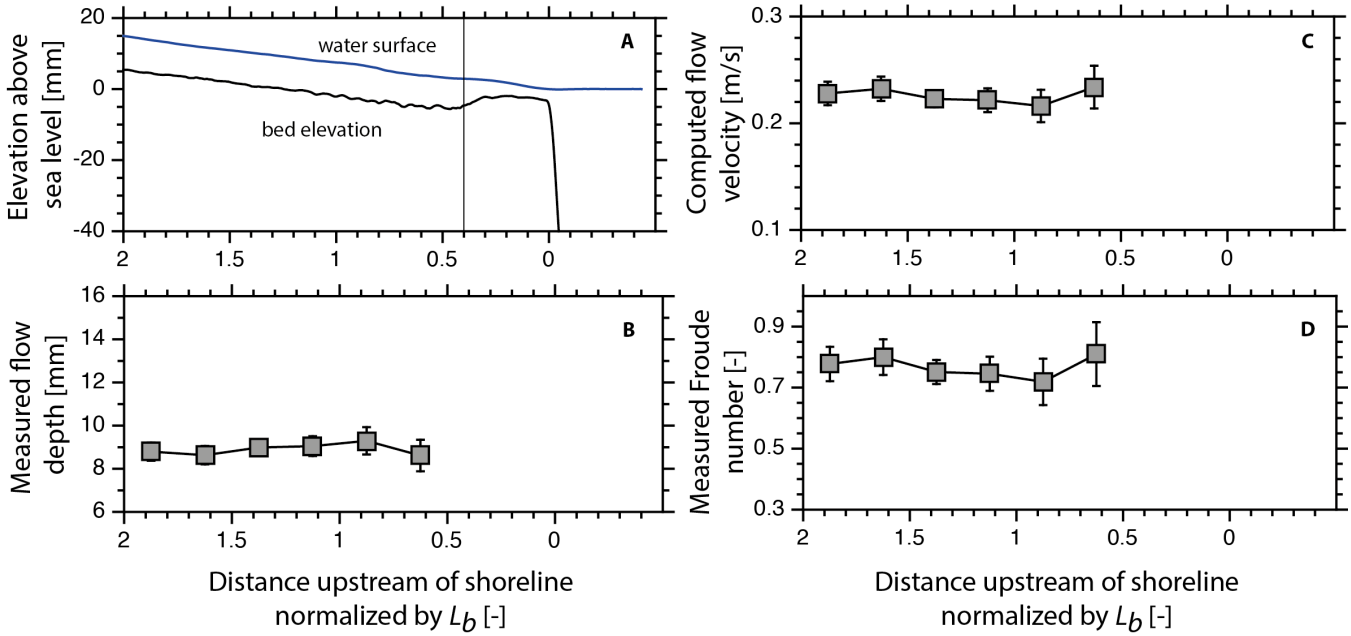


**fig. S2. Instantaneous measurements of water and bed surface profiles along with the measured flow depth, depth-averaged flow velocity, and Froude number for experiment A.** **(A)** Long profiles of water (blue) and bed (black) surface measured along the centerline of the flume at an experimental runtime of 7.6 hrs. The vertical black line indicates the change in confinement in the experimental facility and downstream of this location the river widened resulting in an adverse bed-slope. **(B)** Measured flow depth computed by differencing the water surface profile and the bed surface profile within the confined portion of the experimental facility. **(C)** Depth-averaged flow velocity computed as the ratio of unit water discharge and measured flow depth in the narrow section of the experimental facility. **(D)** Computed Froude number using the depth-averaged flow velocity and the measured flow depth within the confined portion of the experimental facility. The data were averaged over a spatial distance of  $0.25L_b$  (0.375 m) and the vertical lines indicate standard deviation. The instantaneous measurements shown here are in good agreement with the time-averaged quantities reported in Table 1.

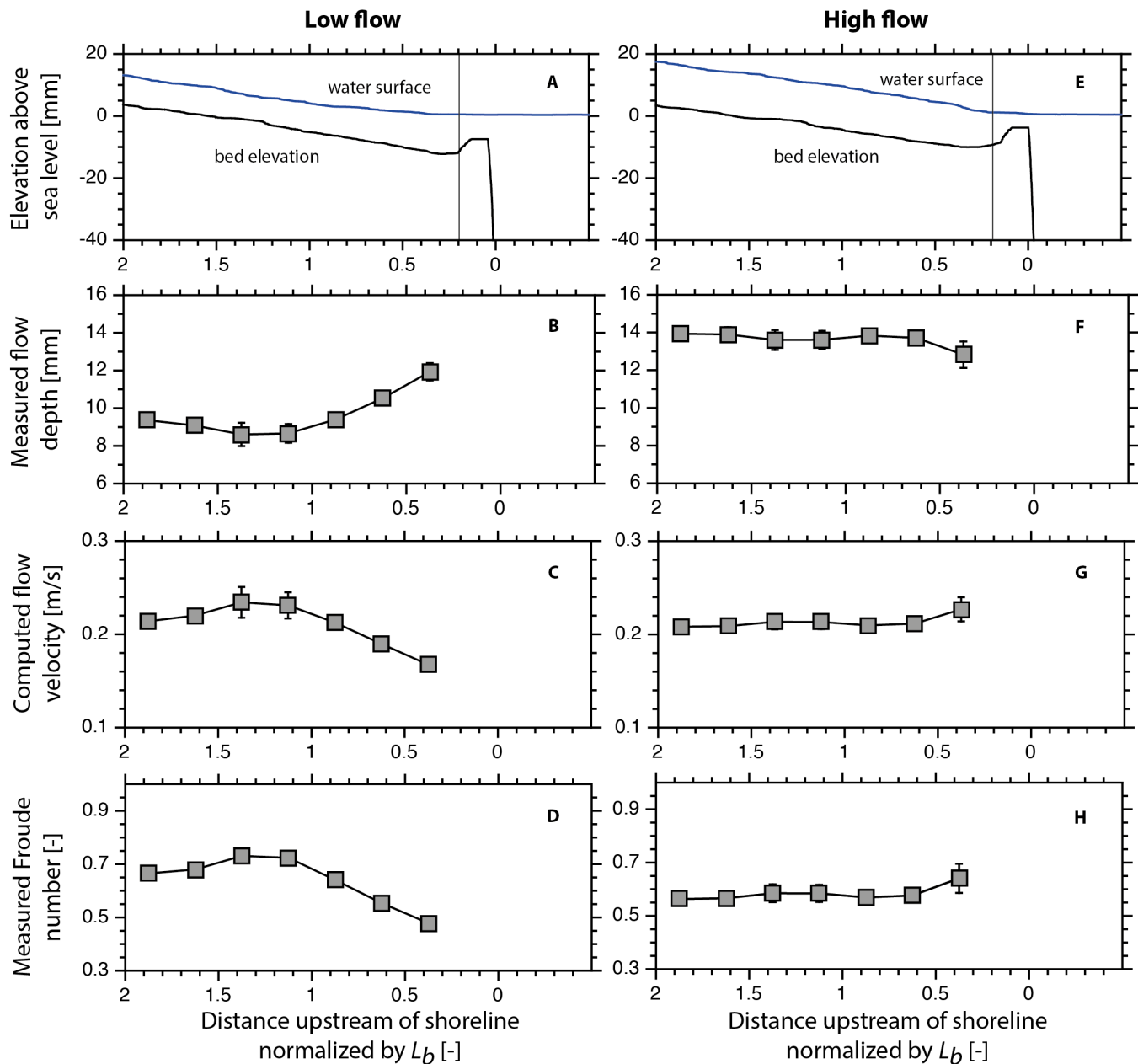


**figure S3. Instantaneous measurements of water and bed surface profiles along with the measured flow depth, depth-averaged flow velocity, and Froude number for both flows in experiment B. (A, E)** Long profiles of water (blue) and bed (black) surface measured along the centerline of the flume at an experimental runtime of 3.8 hrs (low flow) and 4.48 hrs (high flow). The vertical black line indicates the change in confinement in the experimental facility and downstream of this location the river widened resulting in an adverse bed-slope. **(B, F)** Measured flow depth computed by differencing the water surface profile and the bed surface profile within the confined portion of the experimental facility. **(C, G)** Depth-averaged flow velocity computed as the ratio of unit water discharge and measured flow depth in the narrow section of the experimental facility. **(D, H)** Computed Froude number using the depth-averaged flow velocity and the measured flow depth within the confined portion of the experimental facility. The data were averaged over a spatial distance of  $0.25L_b$  (0.72 m) and the vertical lines indicate standard deviation. The instantaneous measurements shown here are in good agreement with the time-averaged quantities reported in Table 1.

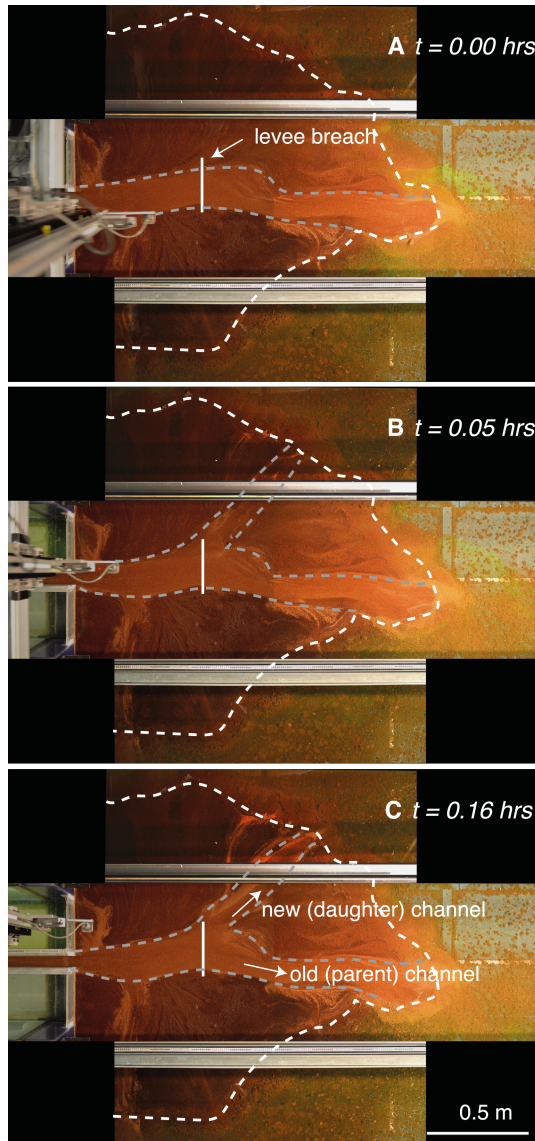


**fig. S4. Photo sequence of the process of avulsion in experiment B.** We picked the avulsion location as the site of the levee breach that resulted in an avulsion. **(A)** The location of the avulsion site that was picked for the example shown in Fig. 3. **(B, C)** These photographs show the creation of the new channel during the course of the high flow event in experiment B. The solid white line is at the same distance from the change in confinement indicating that our choice of avulsion site and consequently the computation of the avulsion length can only have an error of a maximum of the channel width. The scale for all the figures is shown at the right corner of panel **C**. Gray and white dashed lines indicate channel banks and the shoreline, respectively.

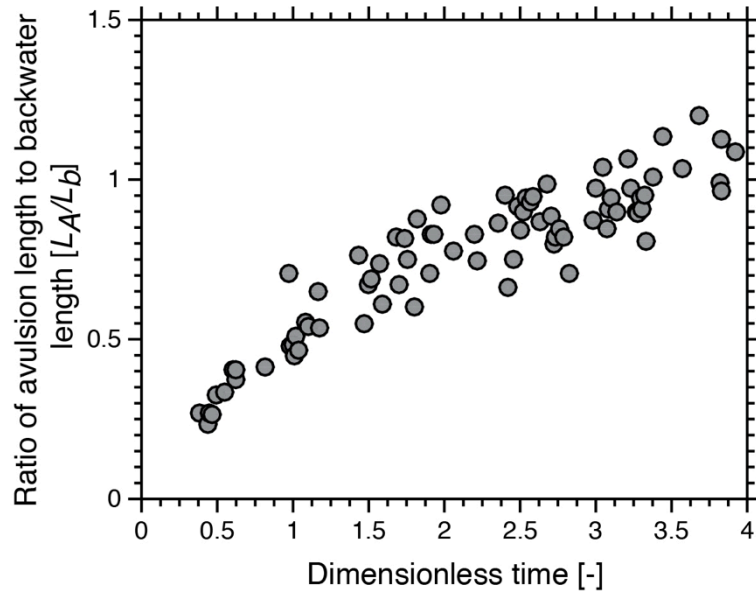


**fig. S5. Temporal evolution of avulsion length in constant discharge delta.** Plot showing the evolution of the ratio of the avulsion length to the backwater length as a function of dimensionless time, where the experimental runtime was normalized by the time it takes to build a radially-symmetric, semi-circular delta of size  $0.5L_b$  (Methods) for the constant discharge delta (Experiment A). In this plot, we show the entire dataset available, which corresponds to approximately a dimensionless time of 4 (Methods). In Fig. 5 of the main text, we show only a subset of the available dataset as the total experimental runtime in experiment B was approximately equal to a dimensionless time of 2.

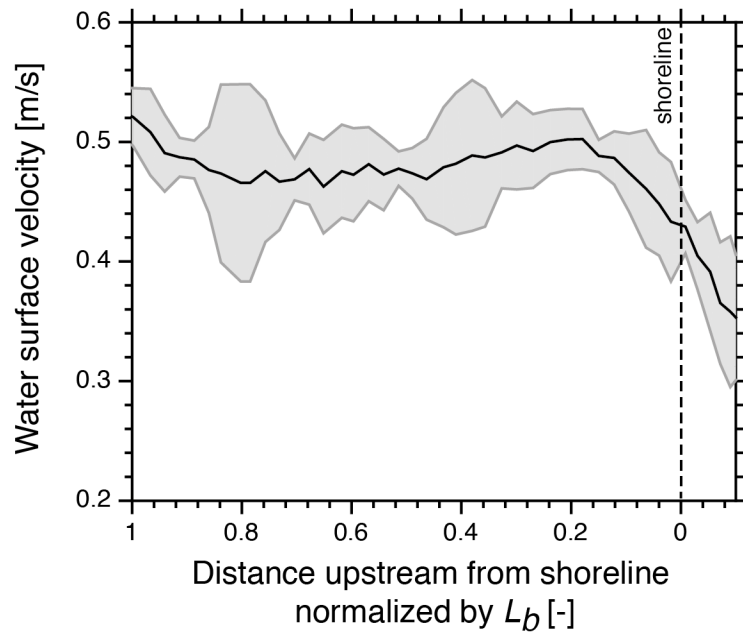


**fig. S6. Water surface velocity across the backwater reach in constant discharge delta.** Plot showing the water surface velocities across the backwater reach for the constant discharge experiment at an experimental runtime of 52.7 hrs when the delta was approximately 1.85 m long along the longitudinal axis of the flume (experiment A). The flow velocity stays relatively constant through the backwater reach (unlike the multiple discharge experiment; Fig. 6B), which indicates that the flow has adjusted to normal-flow conditions through most of the alluvial reach highlighting the transient nature of backwater hydrodynamics in the absence flood variability. The flow velocities were computed using the overhead videos of dye transport and the shaded region indicates standard error arising from window averaging of instantaneous data (Methods).

**table S1. Field data compilation of avulsion length and backwater length.** Table documenting the database of deltaic river characteristics reproduced from *Chatanantavet et al. (18)*, which were used to produce Fig. 1 of the main text.

River	Width (m)	Slope	$Q_c$ (m <sup>3</sup> /s)	$h_c$ (m)	$L_b$ (km)	$L_A$ (km)
Parana	1270	0.00004	22800	11.8	295	210
Danube	1250	0.00005	9700	6.3	125	95
Nile	240	0.000064	8800	16.2	254	210
Lower Mississippi	650	0.000043	29000	21.0	480	490
Rhine-Meuse	700	0.0005	5750	5.0	45.5	51
Magdalena	1100	0.000095	11040	6.0	63.2	67
Orinoco	2000	0.00006	24550	8.0	133.3	78
Mid Amazon	3000	0.00003	47800	12.0	400	404

For the Huanghe, we report values of  $L_A$  and  $L_b$  from *Ganti et al. (15)*. They used historical cross-sections to estimate the bankfull depth of the lower Huanghe, and combining that with the estimated channel bed slope yielded a backwater length scale of 21-54 km (15). Huanghe historically avulsed on decadal timescales and the avulsion length was variable and the mean and standard deviation of the avulsion length was  $31 \pm 10$  km (15). Because avulsion sites on the Huanghe translated downstream, we report a scale bar showing the avulsion length instead of tracing the channel from the shoreline to the avulsion node in Fig. 1 of main text.

We also note that the backwater length scale is a scaling parameter that determines the length scale over which the alluvial river feels the boundary condition of the sea level. The actual length scale over which the hydrodynamics of the river are affected by the boundary condition varies with both the Froude number and the ratio of the normal flow depth to the depth of flow at the river mouth (e.g., 20, 54). *Bresse* (54) and *Lamb et al.* (20) showed analytically that the minimum length scale over which backwater hydrodynamics prevail is  $L_b$  while the maximum length scale over which drawdown hydrodynamics prevail is  $0.5L_b$ . Thus, the correlation of backwater length scale and the measured avulsion length is an indication that backwater hydrodynamics play an important role in setting the location of river avulsions on deltas.

**Supplementary Video captions:**

**movie S1. Experimental evolution of constant discharge delta.** This video shows the temporal evolution of constant discharge delta (experimental delta A). The video was made using the overhead images of deltaic evolution with a temporal resolution of 1 min. One second of video time corresponds to one hour in real time and the length of the silver rails is approximately 1.6 m.

**movie S2. Experimental evolution of variable discharge delta.** This video shows the temporal evolution of variable discharge delta (experimental delta B). The video was made using the overhead images of deltaic evolution with a temporal resolution of 1 min. One second of video time corresponds to one hour in real time and the length of the silver rails in the image is approximately 1.6 m.

**movie S3. Overhead dye video of the constant discharge delta.** This overhead video shows fluorescent dye transport captured at a rate of 59 fps at an experimental runtime of 52.7 hrs in experiment A. The width of the confined portion of the alluvial river section is 7 cm.